The 7th International Supercritical CO_2 Power Cycles Symposium
March 31 – April 2, 2020, San Antonio, Texas
Paper #

First demonstration of PIV measurements in sCO_2 flows inside microchannel near the critical point

Anatoly Parahovnik, Suhyeon Park, Yoav Peles, and Subith Vasu
Mechanical and Aerospace Engineering, University of Central Florida, Orlando, FL 32816, USA,
Yoav.Peles@ucf.edu; subith@ucf.edu

ABSTRACT

Particle image velocimetry (PIV) enables researchers to measure flow filed and turbidimetric energy of a flow without disturbing it. This technique is commonly used in both in macro and micro scale experiments. In this work, PIV capabilities were expanded to enable measurement at pressure close to the critical conditions of CO_2. To our best knowledge, though this preliminary work is meant to demonstrate that PIV can be applied, this is the first PIV measurements in CO_2 flows at microscale for these high pressure conditions. Such data will enable to achieve valuable flow characteristics and heat transfer correlations of near critical and supercritical CO_2 flows.

INTRODUCTION

Particle image velocimetry is an optical measurement technique for flow visualizations. Figure 1 shows configuration of setup and procedures of *PIV* measurement [1].

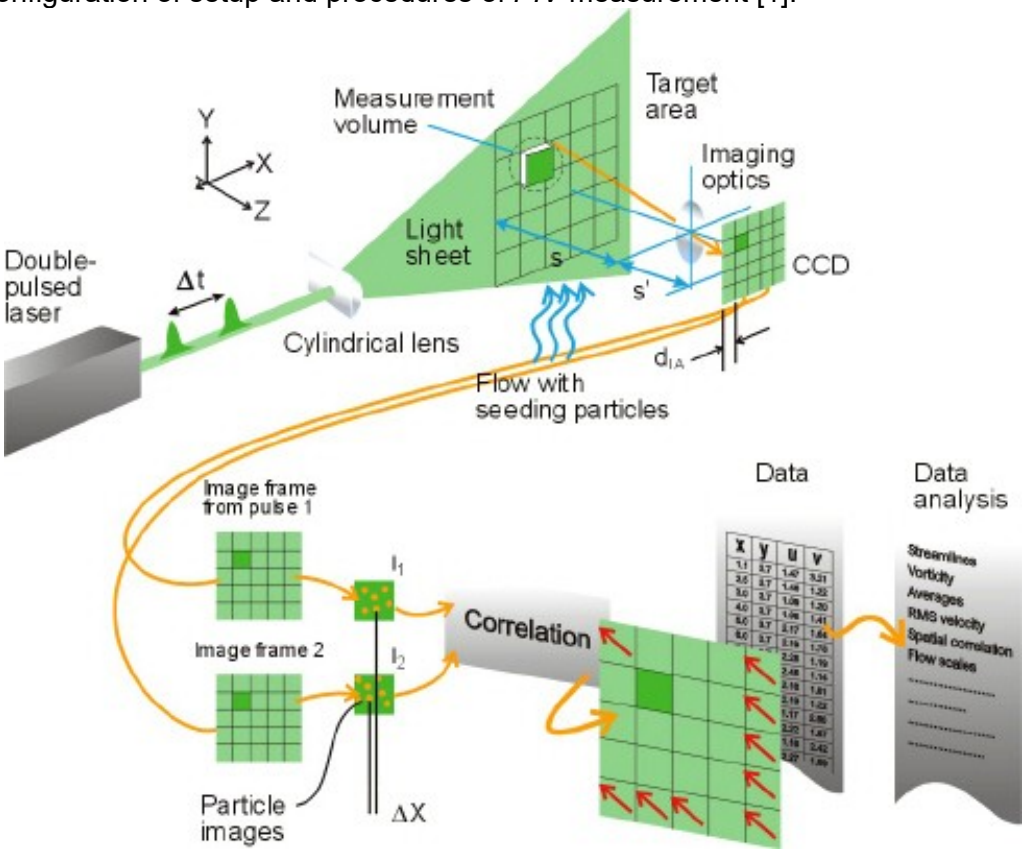

Figure 1: Principle of particle image velocimetry [1].

Two images are compared with a predetermined time delay, and then the difference between the images is analyzed to obtain velocity vectors from shift of particle locations. Planar *PIV* is the most common configuration, which uses a single double-shutter camera. A *PIV* system comprises of a seeding system, a double pulsed laser, sheet optics, a charged coupled device (*CCD*) or *CMOS* camera, a timing unit, and a software. Laser light is projected into a thin light plane guided into the flow medium by sheet optics. Small sized particles submerged in the flow in motion are illuminated by a laser sheet. For solid particle seeding, a cyclone seeder or a nebulizer can be used. The camera captures the particle images in the measurement plane within the thickness of the laser sheet. After cross-correlation and accompanied image processing, 2D velocity vectors are obtained.

First, pair of images are obtained with a time delay Δt. Cross-correlation is performed in each interrogation area as shown in Eq. 1. Peak of the cross-correlation is searched followed by subpixel interpolation. Finally, velocity vector is obtained in each interrogation area. Figure describes the cross-correlation in a spatial domain.

$$R_{II}(x,y) = \sum_{i=-K}^{K} \sum_{j=-L}^{L} I(i,j)I'(i+x,\, j+y) \qquad (1)$$

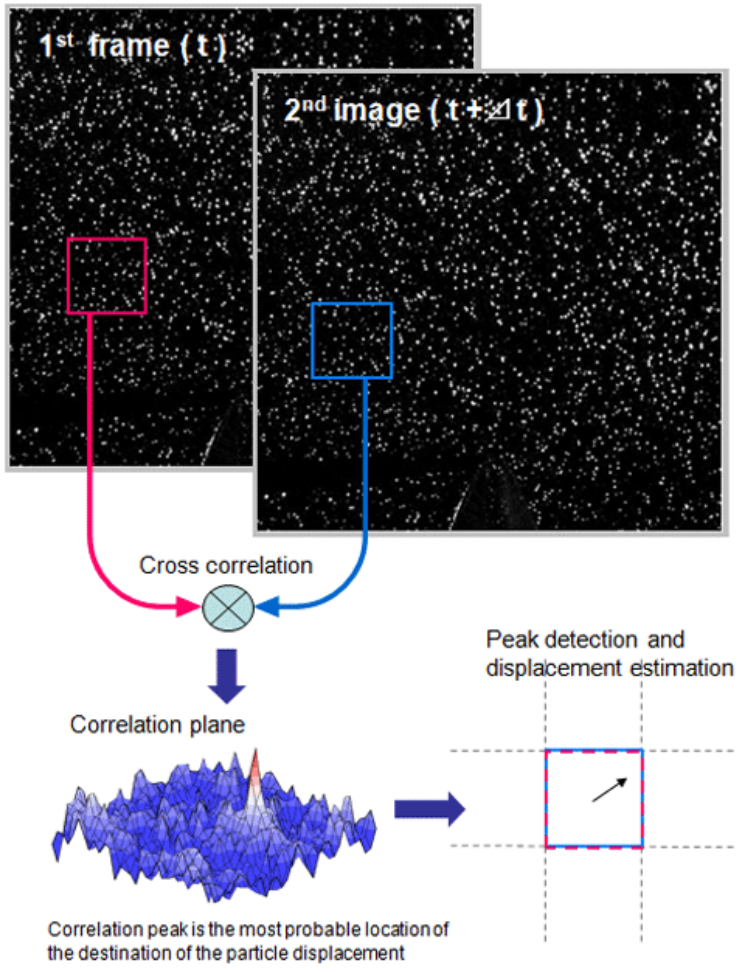

Figure 2: Example of cross-correlation of raw images in interrogation area [2].

Relaxation time of particles, defined as τ_s (Eq. 2) provides a measure of the capacity of the seeding particles to follow the fluid [3]. The relaxation time needs to satisfy the required time response by selecting appropriate particle size to represent the flow field from the seed particles velocities. Relaxation time increases when flow viscosity decreases. Therefore, smaller particle should be used for low viscosity flow.

$$\tau_s = \frac{d_{particle}^2 \rho_{particle}}{18\mu_{fluid}} \qquad (2)$$

Synchronization between the laser and the camera is precisely controlled by a timing unit. Specialized *PIV* cameras are capable of taking pairs of images with a short time delay. Typically, time scale of the delay of image pairs is a micro second. Time duration of laser pulse is much shorter than the exposure time of the camera sensor. Figure 3 shows how timing control signal works.

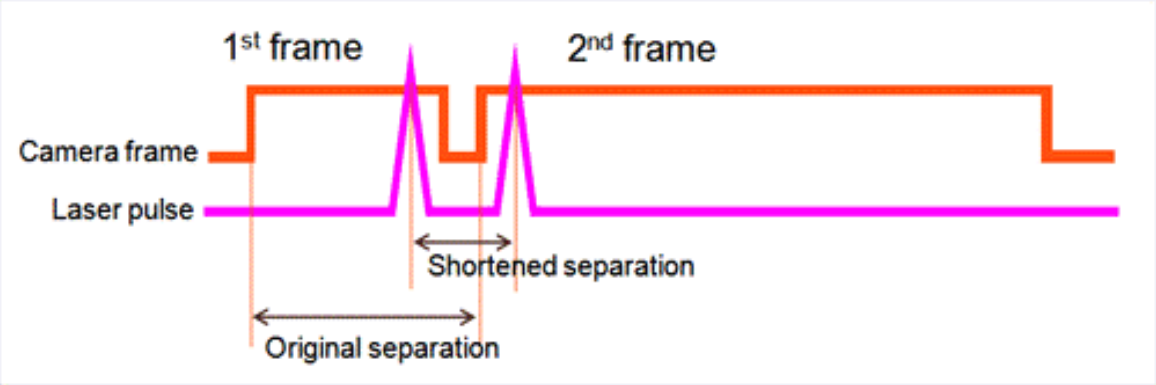

Figure 3: Timing signals for laser and camera synchronization [2].

Image processing software is provided by the distributor of the *PIV* system. The image processing includes background removal, normalization, adaptive cross-correlation, sub-pixel interpolation, and removal of invalid vectors. The mean velocity field is obtained from *PIV* measurements. The arithmetic mean of the snapshots ($\overline{v}$) is called the mean vector field.

Micro-*PIV* systems are designed to measure flow fields on microscopic scales using dedicated microscopic imaging components. The light sheet applied in planar *PIV* applications is replaced by a volume illumination of the flow, and the depth of field is determined by the numerical aperture of the objective lens of the microscope. Flow seeding fluorescent particles are used to remove the strong background light from nearby surfaces. The fluorescent light is red-shifted from the excitation light and separated using a filter cube [4].

Two distinct flow regimes, laminar and turbulent, are of interest. The former is more settled and predictable while the latter is more uncertain. Proper classification of flow regime is of great importance for correct treatment and analysis of the flow. The transition between the regimes is usually defined by the Reynolds number (*Re*). For external and internal flows, the transition Reynolds number between laminar and turbulent are 10^5 and 2300, respectively. The thermophysical properties of CO_2 near the critical conditions varies considerably. These variations introduce challenges for simulation and for in-depth analysis of the flow regimes and flow patterns.

The authors have constructed a set up to obtain velocity fields in supercritical CO_2. The current system allows to measure the local wall temperature inside the microchannel and to obtain high-speed synchronized (to the surface temperature reading) images.

EPRERIMENTAL FLUIDIC SETUP

The experimental setup consisted of a microdevice, its package, a pneumatic flow system, and a sampling system.

A. Micro device

Having superior mechanical properties than more common barefoot glass, fused silica was used to make the micro device; it allowed a visual access into the flow.

The device was made of two parts pressed to each other. The top piece (see Fig. 4), which was micro machined with traditional subtractive manufacturing techniques, had 0.7 mm diameter inlet and outlet and rectangular microchannel, channel high was 0.1 mm and its hydraulic diameter was 0.3 mm. A bottom piece is a 0.5 mm thick fused silica plate that was cut into the required dimensions.

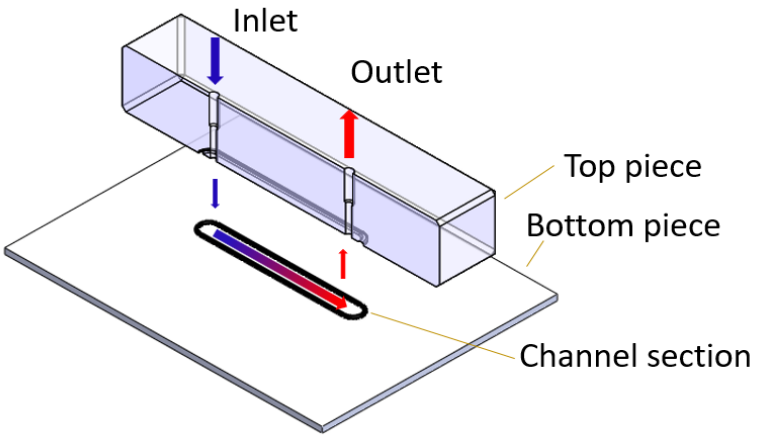

Figure 4- microdevice configuration

B. Package

The package (shown in Fig. 5) housed the microfluidic device. The package delivered the fluid in and out of microfluidic device with standard ¼" compression fittings. When assembled the package press the bottom and top piece at their interface, contact surfaces were polished and formed tight sealing. To evaluate the leakage rate, the assembly was pressurized to 7.4 MPa for 1 hour and no pressure drop were detected. No visible damage was detected or increase in a leakage rate after the assembly was exposed to pressure of 10.4 MPa for 10 minutes as part of a pressure tolerance test. Last, a visualization window was designed to enable optical access into the microchannel

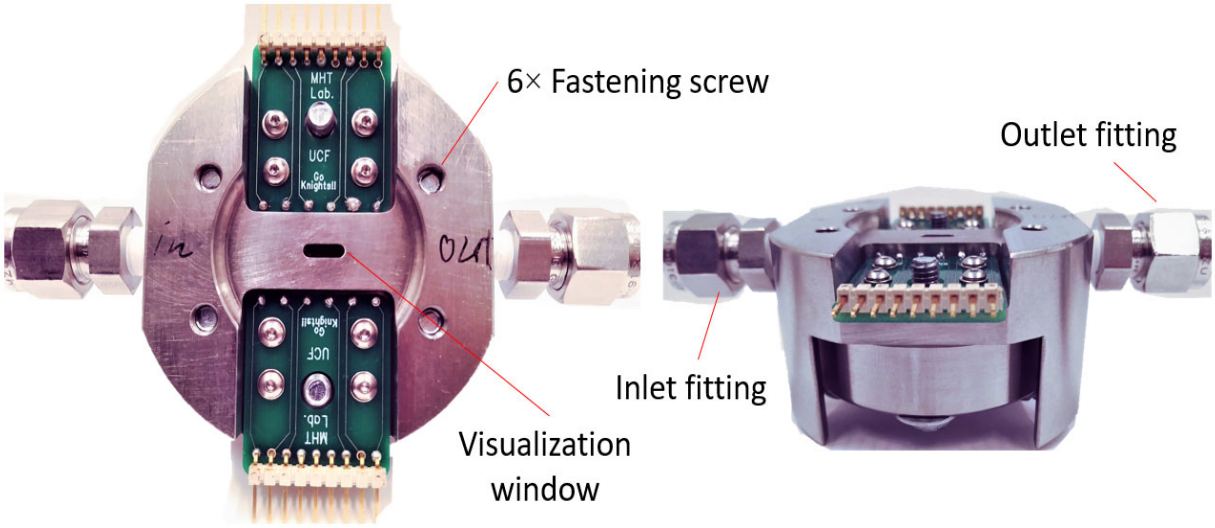

Figure 5-Package that contains the microfluidic device with visualization window and tube fittings

C. Fluid delivery system:

The CO_2 was delivered from a storage tank (Fig. 6) with initial pressure of approximately 6 MPa (point 1), afterwards the flow was introduced into the particle cartridge (point 2a). The cartridge was a straight tube that was filed manually with alumina particles of 3μm size. It had a bypass (point 2b) and a needle valve prior to it, this configuration enabled timing particles into the fluid and rough control of the number of particles that were introduced into the flow. The control was done by opening and adjusting the needle valve, this configuration enabled the performance of experiments with and without particles. At the next step, the flow was sampled inside the microfluidic device using a microscope connected to high speed camera for the PIV measurement (point 3). To control the flow rate, a needle valve was placed after the microfluidic device (point 4), the valve and its adjoining tubing had to be heated to avoid solidification of the carbon dioxide due to the pressure drop and consequently temperature drop due to Joule – Thomson effect for that purpose a Joule heater that was wrapped around the tube. Finally, the particles were filtered out of the CO_2 by discharging them into a water which trapped the particles (point 5), After filtering a purified CO_2 gas was released into the ambient from a sealed vessel that encapsulated the water (point 6).

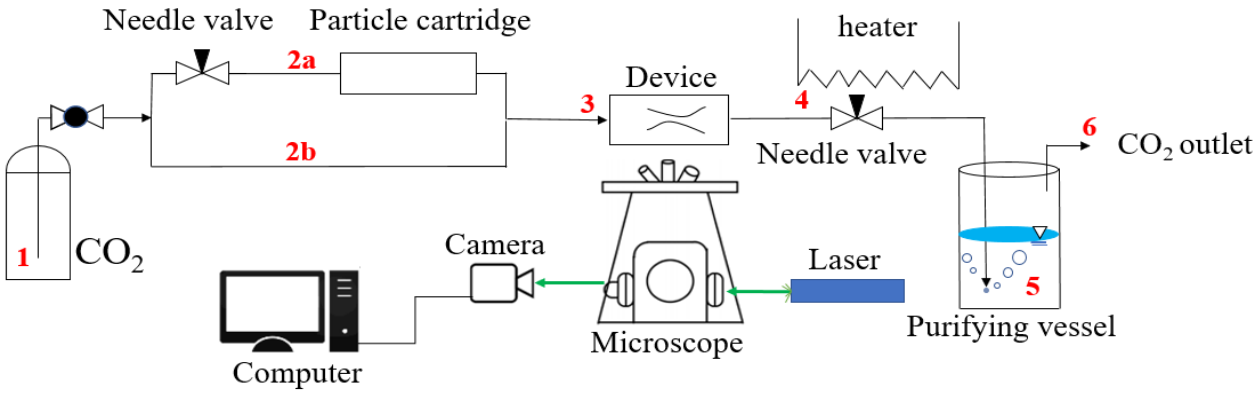

Figure 6 Fluid delivery system experimental setup

PRELIMINARY RESULTS

A dual cavity laser (laser power was set to minimum ~20 mJ) and a slow frame rate (~15 fps) was introduced through a light source port on the microscope. Data was collected in Andor's software and output TIF images were processed in LaVision's® software. Particle displacement was ~500 px at initial attempt with 8 µs delay (time between pulses). Light intensity at the particle location is reduced by scattering while background is illuminated relatively uniformly.

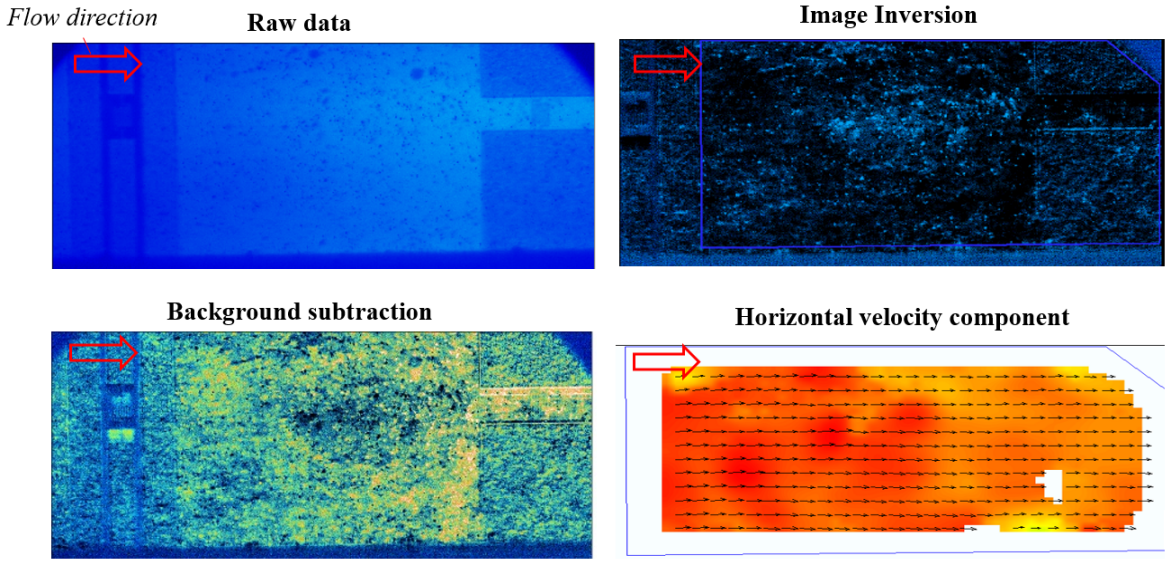

Figure 7- Horizontal velocity vector that was obtained through the PIV analysis

Alumina particles were introduced into near critical pressurized CO_2 flow in a microchannel. After being exposed to pressurized CO_2 for 3 days, they were found to be inert to CO_2. The uniformity of the seeding can further be improved by more structured and controlled partials seeding process. Nevertheless, the flow was captured in an adequate way (Fig. 7) and its velocity was recorded. Velocity of a particle that was obtained using PIV analysis was 30-50 m/s that is consistent with the first principles calculation.

ACKNOWLEDGEMENTS

This material is based upon work supported by the Office of Naval Research (ONR) under award number N00014-18-1-2362.Partial financial support from UCF College of Graduate Studies is appreciated. The authors thank Akshay Khadse and Dr. Erik Fernandez (both UCF) for their help with the PIV set up.

REFERENCES

[1] DantecDynamics, 2019, "https://www.dantecdynamics.com/measurement-principles-of-piv."
[2] Seika, 2019, "https://www.seika-di.com/en/measurement/principle_of_piv.htm."
[3] Ji, J., and Gore, J. P., 2002, "Flow structure in lean premixed swirling combustion," Proceedings of the Combustion Institute, 29(1), pp. 861-867.
[4] LaVision, 2019, "https://www.lavision.de/de/applications/fluid-mechanics/index.php."